

The hydrodynamic torque dipole from rotary bacterial flagella powers symmetric discs

Received: 25 April 2025

Accepted: 19 January 2026

Published online: 27 March 2026

 Check for updatesDaniel Grober¹, Tanumoy Dhar², David Saintillan² & Jérémie Palacci¹✉

Swimming bacteria move through a fluid by actuating their moving body parts. They are force-free and can be described as hydrodynamic force dipoles: pushers or pullers. This modelling description is broadly used in biological physics and active matter research, and it has successfully predicted, for example, the superfluid behaviour of suspensions of pushers or the bend instability and emergence of turbulent flows in active nematics. However, this description accounts only for the translational motion of the swimming body and neglects the effects of hydrodynamic torque dipoles, which are relevant to bacteria with rotary motor-driven flagella, such as swimming *Escherichia coli*. Here we show that the torque dipole of confined swimming *E. coli* can power the persistent rotation of symmetric discs. The torque dipole leads to a traction force on the discs, an additive mechanism that is both contactless and independent of the orientation of the bacteria. Our results indicate that the torque dipole of swimming *E. coli* is notable in confined geometries, which is relevant to bacterial transport through porous materials, biofilms and the development of chiral fluids.

Motile bacteria are micrometre-sized, self-propelling machines that convert biochemical energy from carbon and oxygen sources into mechanical work and motion. Owing to the kinematic reversibility of motion at low Reynolds numbers, the propulsion mechanism must break time-reversal symmetry to achieve a net displacement¹. For *Escherichia coli* bacteria, this is achieved with the actuation of flagella by the proton-driven bacterial flagellar motor (BFM)², whose persistent rotation propels the bacteria forward^{3,4}. This results in the transfer of mechanical work from the bacteria to the fluid, which takes the surrounding medium out of equilibrium and is effectively an active bath. This leads, for example, to an increase in the diffusivity of colloidal spheres controlled by the activity of the bacteria^{5–8}. Notably, in an apparent departure from equilibrium physics, bacterial baths have been used to power microgears, provided they have asymmetric shapes^{9–11}. In these experiments^{9,10}, symmetric gears simply fluctuate, whereas asymmetric gears display persistent rotation, whose direction is controlled by the geometry¹². This strategy has been replicated

with active colloids nested in asymmetric gears¹³ and used to control the propulsion of objects in bacterial baths^{14–17}. The rotation in these examples results from the rectification of the forces exerted by the bacteria as they push against the walls, following pioneering work on bacteria tethered to a microrotor¹⁸.

Moreover, we recently demonstrated that colloidal aggregates exhibit persistent rotation when immersed in a suspension of swimming *E. coli*. We reported that the direction of rotation was controlled by the slip conditions of the interface where the aggregates sit. Colloidal aggregates rotate clockwise on the no-slip surface of a glass capillary and anticlockwise on an air–water interface, reminiscent of the change of direction of rotation of swimming *E. coli* on interfaces¹⁹. In effect, suspensions of swimming *E. coli* constitute chiral active baths that transmit torque to colloidal aggregates and, ultimately, control the formation of unconventional gels²⁰.

Colloidal aggregates, however, form from random collisions and, thus, lack the shape asymmetry required in refs. 9,10,12. This

¹Institute of Science and Technology Austria, Klosterneuburg, Austria. ²Department of Mechanical and Aerospace Engineering, University of California, San Diego, San Diego, CA, USA. ✉e-mail: jeremie.palacci@ista.ac.at

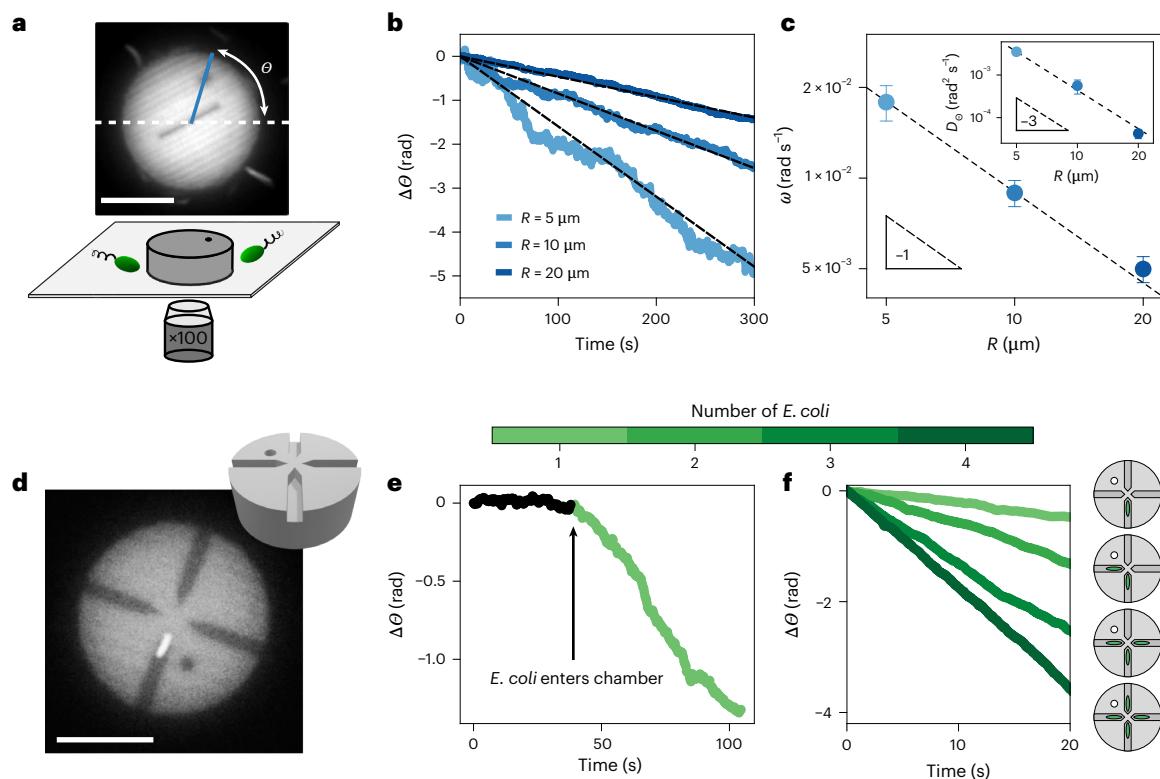


Fig. 1 | Dynamics of colloidal pucks in a bath of swimming *E. coli*.

a–c. Collisions from *E. coli* swimming clockwise rotate symmetric discs ($\rho_B = 6 \times 10^8$ cells per millilitre). **a**, Bottom: schematic of the experiment. Nanoprinted discs (dubbed ‘pucks’) are immersed in a bath of swimming *E. coli* bacteria. Top: fluorescence microscopy image of a puck and the definition of its orientation θ . **b**, Dynamics of pucks, $\theta(t)$, for radii $R = 5 \mu\text{m}$ (light blue), $10 \mu\text{m}$ (blue) and $20 \mu\text{m}$ (dark blue). All pucks exhibit a slow clockwise rotation. A linear fit gives the average rotation rate ω (dashed black lines). **c**, Puck rotation rate ω . Insets: rotational diffusivity D_0 for pucks of different sizes, measured from the mean squared angular displacement (Supplementary Information). The triangles indicate a slope of -1 (main panel) and -3 (inset). Data symbols with error bars represent the average and standard deviation for

pucks with the same radius $R = 5 \mu\text{m}$ ($N = 6$), $10 \mu\text{m}$ ($N = 7$) and $20 \mu\text{m}$ ($N = 4$). **d–f.** *E. coli* in confinement power symmetric discs ($\rho_B = 3 \times 10^7$ cells per millilitre). **d**, Fluorescence microscopy image of a puck with four chambers, each ending near the centre of the disc, as visible from the 3D design (inset). The chambers are $2 \mu\text{m}$ in height and $2 \mu\text{m}$ in width. A GFP-labelled *E. coli* is visible in the lower chamber. **e**, At the present concentration, the puck barely rotates until an *E. coli* enters the chamber, leading to a drastic increase in the clockwise rotation, which persists as long as the bacterium occupies the chamber. **f**, Dynamics of rotation $\Delta\theta(t)$ for pucks containing different numbers of trapped *E. coli* (see schematics on the right). The pucks all rotate clockwise, with rates increasing with the number of bacteria. Scale bars, $10 \mu\text{m}$.

raises the question of whether bacterial baths can power the persistent rotation of objects in the absence of shape asymmetry. To investigate this, we leverage state-of-the-art three-dimensional (3D) nanoprinting and study the dynamics of symmetric microdisks, dubbed ‘pucks’, immersed in suspensions of motile *E. coli* (Fig. 1a). We, thus, identify a new mechanism for the transduction of torque from the rotary motor-driven flagella towards objects in their surroundings. Here we show that the BFM of swimming *E. coli* exert a torque dipole and a traction force that leads to the rotation of even symmetric objects. This hydrodynamic mechanism is contactless and relies on confinement rather than the shape asymmetry of the gears, thus contrasting with previous work on micromachines powered by bacteria or active colloids^{9,10,12}. Our findings highlight the importance of the bacterial hydrodynamic torque dipole in confinement. The implications for dense and confined suspensions need to be investigated.

Results

Bacteria are torque dipoles and swim in circles

As our observations were performed near the bottom of a glass capillary, where objects are confined by gravity, we first recapitulate the swimming behaviour of swimming *E. coli* near a no-slip wall. Swimming *E. coli* are force- and torque-free. They are accurately represented hydrodynamically by a force dipole²¹ and a torque dipole: the flagella

spinning one way and the body spinning the other way to balance the torque. In effect, swimming *E. coli* are hydrodynamically attracted to solid walls by the image charge of the force dipole²² and swim in (clockwise) circles as a result of the opposing shear forces induced by the torque dipole²³ (Supplementary Fig. 2a).

Experimental procedure

We now study the dynamics of 3D-printed discs, dubbed ‘pucks’, in the presence of swimming bacteria. The pucks were printed with radius $R = 5 \mu\text{m}$, $10 \mu\text{m}$ or $20 \mu\text{m}$ and constant height $\sim 6 \mu\text{m}$ using a two-photon-polymerization printer (NanoOne, UpNano) (Fig. 1a and Supplementary Information). After printing and development, they were dispersed in a solution of 5% F 108 surfactant to prevent aggregation and were subsequently concentrated (Supplementary Fig. 1). The pucks were added to a suspension of swimming *E. coli* in a motility medium and sealed in a glass capillary (Methods). The concentration of swimming *E. coli* (ρ_B) was adjusted before the experiment and is described in each section. The pucks sedimented. They sat at the bottom of the capillary and interacted with swimming *E. coli* (Fig. 1a). We carried out our observations by fluorescence microscopy using the autofluorescence of the nanoprinting resin and the green fluorescent protein (GFP) tag of the bacteria (Supplementary Information). A dot and a line were added to the design so that we could track the orientation $\theta(t)$ of the pucks (Fig. 1a).

Collisions with *E. coli* swimming clockwise rotate symmetric discs

We first observed the dynamics of simple pucks—thick discs—in a bacterial bath of concentration $\rho_B = 6 \times 10^8$ cells per millilitre. The clockwise rotation of aggregates was observed in ref. 20. Bacteria did not cross underneath the discs, as visible from fluorescence microscopy. They collided with the perimeter of a puck and deflected (Supplementary Video 1 and Supplementary Fig. 2b). The discs exhibited noisy dynamics at short times, reminiscent of the high effective temperature of the bacterial bath^{5–7,20} (Fig. 1c inset and Supplementary Fig. 3). Over the course of minutes, the pucks displayed a slow but perceptible clockwise rotation for all tested radii $R = 5 \mu\text{m}$, $10 \mu\text{m}$ and $20 \mu\text{m}$ (Fig. 1b). We quantified these observations by tracking the angle $\theta(t)$ (Fig. 1a) and computing the rotation rate ω_R of the pucks from a linear fit of $\theta(t)$. We found that $\omega_R \propto 1/R$ (Fig. 1c), as previously found for colloidal aggregates in bacterial baths²⁰. In brief, the curved trajectories of the swimming bacteria, as exemplified in Supplementary Fig. 2, lead to asymmetric collisions with the puck. These collisions produce a net torque and persistent rotation, in the absence of shape asymmetry (see ref. 20 for details of this toy model and Supplementary Section 2). The rotation is driven by forces on the perimeter of the disc, a mechanism akin to conventional bacterial machines (for example, see refs. 9,10,12,16,17), whereby a shape asymmetry was used to rectify the motion of *E. coli* and power rotation. In the present experiment, the asymmetry arises from the chirality of the clockwise trajectories of the *E. coli* swimming above the solid interface of the glass capillary.

We estimate the effective tangential force F resulting from collisions of the puck with swimming bacteria as $F^* = \frac{\omega}{M_{\theta}R} \approx 0.006\text{--}0.06$ pN, based on the reported rotation rate $\omega \approx 10^{-3}\text{--}10^{-2}$ rad s^{-1} (Fig. 1c) and independent measurements of the rotational mobility M_{θ} of the puck (Supplementary Fig. 4). This value of F is markedly smaller than the effective pushing force per cell measured for micromotors powered by swimming *E. coli*, $F \approx 0.2$ pN (ref. 12), as well as the typical flagellar thrust of *E. coli* cells^{21,24}. This reflects the minimal rectification proportional to ℓ_B/R_c arising from the collisions of the curved trajectories with the puck perimeter, where $R_c \approx 50 \mu\text{m}$ is the radius of curvature of the trajectories and ℓ_B the bacteria length, as discussed in Supplementary Section 2. The effect is, however, sufficient to drive persistent rotation over long timescales and control unconventional aggregation²⁰. Notably, our simple model satisfactorily predicts the observed rotation rate when accounting for the collision rate observed in the experiment (Supplementary Section 2).

E. coli in confinement power symmetric discs

In this section, we present a new type of bacterial machine, one that is powered by the torque dipole of individual *E. coli* confined beneath symmetric discs. The effect is contactless, as it does not have the aforementioned collisions that power conventional bacterial ratchets. Here we present the experimental evidence that led us to unveil this new physical mechanism. We introduce two variants of the circular pucks, each with fixed radius $R = 10 \mu\text{m}$. Our aim was to confine individual *E. coli* underneath them. The first kind is a disc with four narrow chambers, placed radially, each terminating near the centre of the puck (Fig. 1d). The second kind has a single narrow channel, open on both ends, along the diameter of the puck (Fig. 2d). We present observations only of pucks where the chambers or channel lie on the bottom substrate, facing down. For the quantitative observations, we suspended the pucks in a dilute bacterial bath ($\rho_B = 3 \times 10^7$ cells per millilitre) and investigated their dynamics as they interacted with individual *E. coli*. Time-lapse data were acquired by spinning-disc confocal fluorescence microscopy (Nikon TI-2 Eclipse, 10 frames per second; Methods). These data were analysed to record simultaneously the position of the centre of mass of the puck, its orientation θ and the position of an *E. coli* body confined beneath the puck. Note that only the body of each bacterium

was fluorescently labelled and that the flagellum, a floppy tail of length $\approx 6.5 \mu\text{m}$ (ref. 25), is not visible in the experiments.

We begin by describing the dynamics of the pucks with chambers following the entry of an *E. coli* into the chamber. The puck has four chambers, each with a square cross section ($2 \mu\text{m} \times 2 \mu\text{m}$), placed radially and ending at a distance $d \approx 0.5 \mu\text{m}$ from the centre of the disc (Fig. 1d). The chambers are large enough for an *E. coli* to enter but too narrow for it to reverse direction; effectively, the *E. coli* becomes confined underneath the puck, while its body and flagella continue to spin. As soon as an *E. coli* positions itself in a chamber, the rotation rate of the puck increases drastically to $\omega \approx 3 \times 10^{-2}$ rad s^{-1} , while always remaining clockwise (Fig. 1e). This was an unexpected finding as the chambers were designed to be radially aligned, thus suppressing any contribution to the torque from direct collisions with the walls. A simple estimate of the rotation rate of a puck arising from a single *E. coli* pushing against the wall of the chamber with force F gives $\omega = M_{\theta}Fd$ (where the lever arm $d \approx 0.5 \mu\text{m}$ is the distance from the dead-end wall of the chamber to the centre of the puck). Thus, $\omega \approx 2 \times 10^{-3}$ rad s^{-1} , an order of magnitude lower than observed in our experiments. We observed marked increases in the rotation rate each time another *E. coli* cell entered one of the other chambers (Fig. 1f). Notably, the fastest rotation rate was observed when there was a bacterium in each of the four chambers (Supplementary Video 2), a situation that should lead to stalling due to the bacteria pushing symmetrically. These results run contrary to previous reports of machines powered by bacteria or active colloids pushing on walls^{9,10,14–17} and require further research.

To elucidate the interplay between bacterial swimming and confinement, we investigated the model situation consisting of a single swimming *E. coli* crossing a puck through an open channel running along its diameter, in the absence of any collisions with the puck perimeter (Supplementary Video 3). In this design (Fig. 2d), there is no wall at the end of the chamber, eliminating the possibility of the bacterium pushing on the end wall. We focused on square channels with cross section $2 \mu\text{m} \times 2 \mu\text{m}$ (Fig. 2), like the chambers used previously. Another geometry with a rectangular cross section is presented in Supplementary Fig. 5.

Swimming bacteria entered the channel and proceeded to exit the puck. The tight confinement prevented them from reversing course. Initially when a bacterium entered the channel, the puck rotated clockwise before eventually reversing direction, leading to a characteristic down–up shape in the dynamics of the puck orientation θ . Notably, this down–up shape did not reverse when a bacterium entered from the other end of the channel (Supplementary Fig. 6). This result shows that the rotation of the puck—always clockwise when the bacterium entered the channel and anticlockwise as it exited—was not set by the direction of navigation of the bacterium.

We quantify our experimental observations by representing the change of angle $\Delta\theta$ of the puck after entry of the bacterium in the channel as a function of the position X_B of the centre of mass of the body of the bacterium in the channel. This representation allowed us to collapse data from bacteria with different swimming velocities (Fig. 2a–d), as expected from low-Reynolds-number dynamics. Indeed, the instantaneousity of the Stokes equations¹ dictates that the net motion of the puck is independent of the rate, that is the velocity, at which bacteria cross the channel. In effect, although bacteria with different swimming speeds (but the same body length, see below) (Fig. 2a) cross the channel in different times (Fig. 2b), the dynamics of the puck collapses when represented as a function of the position of the bacterium in the channel, $\Delta\theta(X_B)$ (Fig. 2c), with a minimum at $X_B \approx 15 \mu\text{m}$ (black dashed line in Fig. 2c). Although the $\Delta\theta(X_B)$ representation effectively collapses the dynamics of rotation of the pucks for similarly sized bacteria with different swimming velocities (Fig. 2a–c), there are noticeable differences in the depth ($\Delta\theta_{\text{max}}$) and position of the minimum for bacteria of different lengths (ℓ_B) (Fig. 2g). Those differences do not correlate

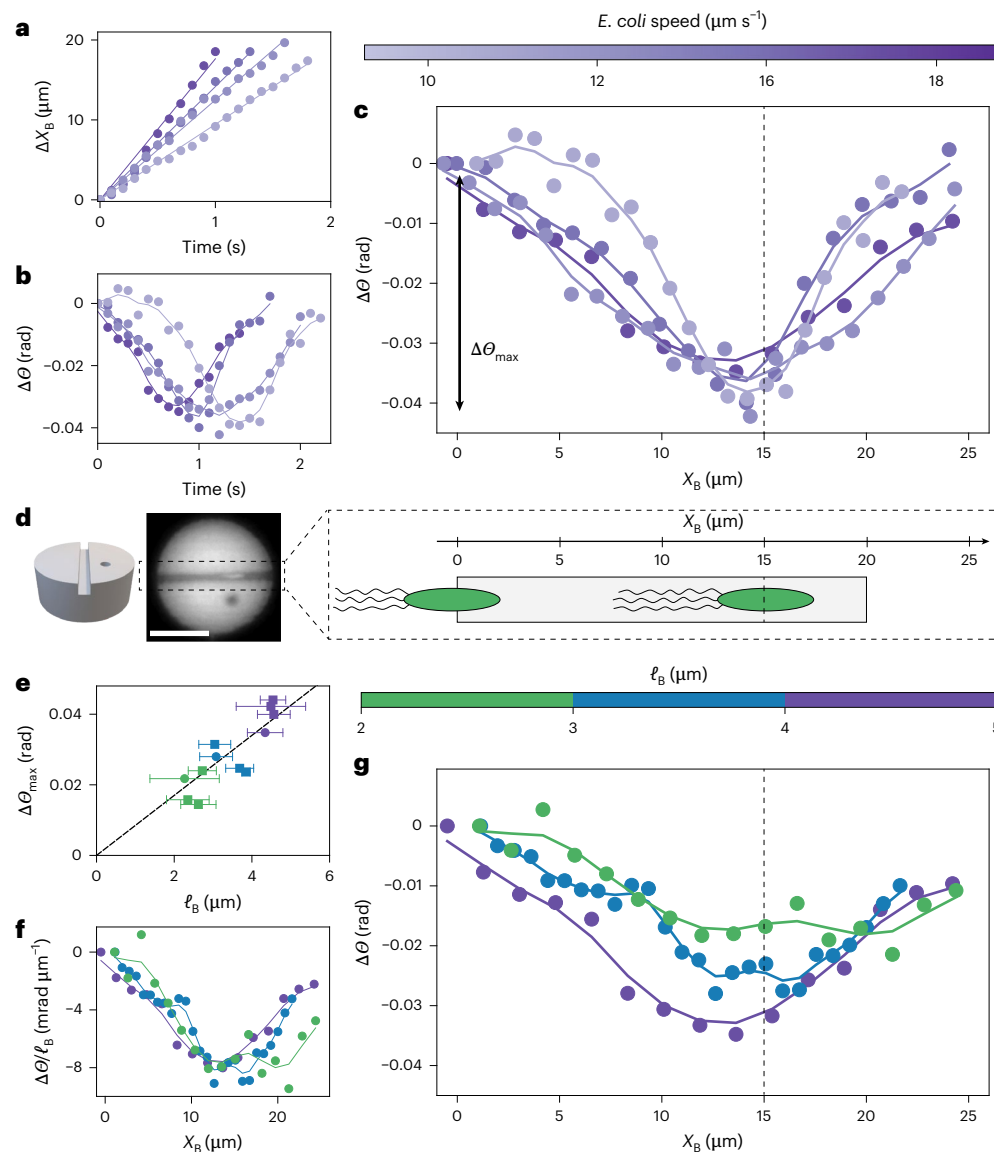


Fig. 2 | Dynamics of pucks with a single swimming *E. coli* crossing the channel.

a, Position of swimming *E. coli* ($X_B(t)$) inside the channel. Different colours indicate different bacteria. The velocity is obtained by a linear fit (solid lines). **b**, Rotation of the puck, $\Delta\theta(t) = \theta(t) - \theta(0)$, as a single swimming *E. coli* passes through the channel. Different colours indicate different bacteria with different velocities (colour bar). **c**, The curves $\Delta\theta(t)$ from **b** collapse when represented as $\Delta\theta(X_B)$, as prescribed by low-Reynolds-number dynamics. $\Delta\theta(X_B)$ decreases before reversing direction, presenting a characteristic ‘down–up’ shape. The dashed line highlights the location of the minimum: $X_B = 2R - \ell_B \approx 15 \mu\text{m}$. The depth of the down–up shape is denoted $\Delta\theta_{\text{max}}$. **d**, Left: schematic of a puck with a single channel. Middle: image of a puck. Right: schematic representation of

E. coli swimming through the channel. The body and flagella are for a puck of radius $10 \mu\text{m}$. The dashed line is the dashed line in **c**. **e**, Depth of the dip, $\Delta\theta_{\text{max}}$, as a function of the body length of *E. coli* (ℓ_B). Each data symbol represents a crossing event by a bacterium ($N = 12$ events). Error bars represent the standard deviation for the bacteria length (ℓ_B) determined by fluorescence microscopy. **f**, Plot of $\Delta\theta(X_B)/\ell_B$ showing the collapse of the first part of the down–up shape, as predicted by the model. **g**, Rotation of the puck, $\Delta\theta(X_B)$, for *E. coli* of different sizes (ℓ_B). The data do not collapse, in contrast to bacteria moving at different speeds (**c**). For larger *E. coli*, the minimum is deeper and occurs earlier. In all panels, solid lines are a Gaussian extrapolation of the experimental data (solid dots). Scale bar, $10 \mu\text{m}$.

with the average angle of the cell body with respect to the channel (Supplementary Fig. 7). Instead, the depth of the dip ($\Delta\theta_{\text{max}}$) correlates with the size of the bacterium body (ℓ_B) (Fig. 2e,f), as quantified by fluorescence imaging of the body. When bacteria with a longer body cross the channel, the dip is more pronounced (with larger $\Delta\theta_{\text{max}}$), and the reversal of direction occurs earlier (X_B is further from the exit).

Hydrodynamic model

The aforementioned observations rule out collisions of the bacteria with the inner channel walls—the driving force behind the rotation of asymmetric gears^{9,10}—as a potential mechanism for the rotation of the pucks with a channel. Instead, we recall that swimming *E. coli*

cells exert a torque dipole on their surroundings, which stems from the counter-rotation of the cell body (clockwise when viewed from the rear) and flagella (anticlockwise), and we intuit that these applied torques lead to the observed phenomenology. The rotation of the body entrains the fluid around it, resulting in a traction field (shear stress) on the walls of the channel. The counter-rotation of the flagella similarly generates an oppositely directed traction field. Because they oppose each other, the two traction fields do not result in a net force on the puck; however, as they are displaced along the channel axis by the effective length of the torque dipole ℓ_D (a distance of the order of the bacterial length), they can apply a net torque to the puck and drive its rotation (Fig. 3a).

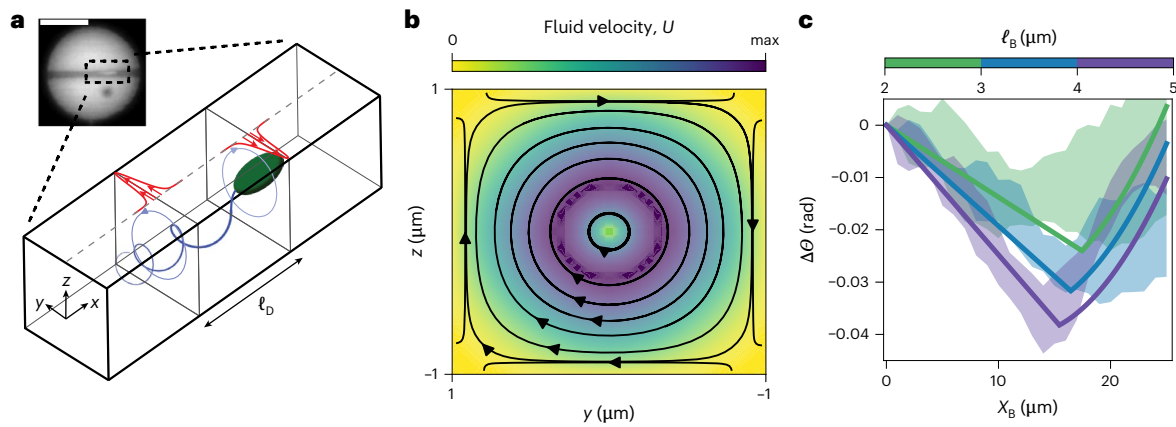


Fig. 3 | Hydrodynamic model of swimming *E. coli* passing through a channel. **a**, Sketch of *E. coli* swimming through a channel. Swimming *E. coli* exert a torque dipole on their surroundings, which stems from the counter-rotation of the cell body (clockwise when viewed from the rear) and flagella (anticlockwise). These two torques drive a hydrodynamic flow resulting in traction forces on the top wall of the channel (red arrows). The traction fields induced by each torque are offset by a distance ℓ_D and, thus, produce a net torque on the puck that drives the observed clockwise rotation. Inset: fluorescence microscopy image of an

E. coli swimming through a channel. **b**, Hydrodynamic flow field from a single, clockwise-rotating rotlet near the front of the bacterium. **c**, Predictions of the model for bacteria of different lengths and, hence, dipole separation ℓ_D (solid lines) and comparison with the experimental measurements. The shaded zones represent the standard deviation of experimental measurements for four trajectories of each size of bacterium. The hydrodynamic model quantitatively captures the experimental observations. Scale bar, 10 μm . max, maximum.

To confirm this mechanism, we modelled the hydrodynamic interaction of a single *E. coli* cell swimming through a square micro-channel of width $2W$. The bacterium is assumed to be aligned with the axis of the channel, consistent with experimental observations. For analytical progress, we approximated the channel walls as infinite stationary boundaries. To leading approximation, the bacterium exerts both a force dipole and a torque dipole on the fluid around it. For a bacterium aligned with the channel axis (x direction), symmetry precludes the force dipole from driving any net torque, and we, therefore, omit it in our flow calculation. Instead, we idealize the bacterium as exerting two equal and opposite point torques (or rotlets) $\pm\Gamma_M \hat{\mathbf{x}}$ at locations $\mathbf{r}_{1,2}$ offset by a fixed distance ℓ_D along the channel axis: $\mathbf{r}_1 - \mathbf{r}_2 = \ell_D \hat{\mathbf{x}}$. The microscopic torque magnitude Γ_M is given by the bacterial motor torque. The torque spacing, or dipole length ℓ_D , is expected to scale with the size of the bacterium, a point we elaborate on below.

We first analyse the effect of a single rotlet $+\Gamma_M \hat{\mathbf{x}}$ at location \mathbf{r}_1 . At low Reynolds number, the fluid motion it induces inside the channel satisfies the Stokes equations,

$$\nabla \cdot \mathbf{U} = 0, \quad \nabla \cdot \Sigma = -\frac{\Gamma_M}{2} \nabla \times [\delta(\mathbf{r} - \mathbf{r}_1) \hat{\mathbf{x}}], \quad (1)$$

where \mathbf{U} is the fluid velocity, $\Sigma = -pI + 2\mu E$ is the Newtonian stress tensor expressed in terms of the pressure p , dynamic viscosity μ and rate-of-strain tensor $E = \frac{1}{2}(\nabla U + \nabla U^T)$, and $\delta(\mathbf{r})$ is the Dirac delta function. The fluid velocity is subject to the no-slip condition at the channel walls: $\mathbf{U}(x, y = \pm W, z = \pm W) = \mathbf{0}$, where the x coordinate is aligned with the channel axis and the z direction is normal to the bottom substrate (Fig. 3a). By linearity of the Stokes equations, the fluid velocity depends linearly on the torque,

$$\mathbf{U}(\mathbf{r}) = \frac{1}{8\pi\mu} R(\mathbf{r} - \mathbf{r}_1) \cdot \Gamma_M \hat{\mathbf{x}}, \quad (2)$$

where $R(\mathbf{r})$ is the Green's function for this problem. As explained in Supplementary Information, the solution for $\mathbf{U}(\mathbf{r})$ can be obtained numerically by solving equation (1) using the boundary-element method²⁶ (Fig. 3b). The velocity field in equation (2) exerts a traction on the channel walls. As the bottom wall is part of the fixed substrate,

only viscous stresses on the top wall ($z = +W$) contribute to the vertical torque on the puck. There, the viscous traction is

$$\mathbf{t}(\mathbf{r}) = -\hat{\mathbf{z}} \cdot 2\mu E(\mathbf{r}) = -\mu \left(\frac{\partial U_x}{\partial z} \hat{\mathbf{x}} + \frac{\partial U_y}{\partial z} \hat{\mathbf{y}} \right), \quad z = +W. \quad (3)$$

This results in a net torque on the puck:

$$\Gamma_1 \hat{\mathbf{z}} = \int_{z=+W} (\mathbf{r} - \mathbf{r}_c) \times \mathbf{t}(\mathbf{r} - \mathbf{r}_1) dS = -(x_1 - x_c) \int_{z=+W} \mu \frac{\partial U_y}{\partial z} dS \hat{\mathbf{z}}, \quad (4)$$

where \mathbf{r}_c denotes the centre of the puck. Upon inserting equation (2), the torque magnitude reduces to

$$\Gamma_1 = -\Lambda \left(\frac{x_1 - x_c}{W} \right) \Gamma_M, \quad \text{where } \Lambda = \frac{W}{8\pi} \int_{z=+W} \frac{\partial R_{yx}}{\partial z} dS. \quad (5)$$

This expression captures the transmission of the viscous torque from the point rotlet (Γ_M) to the puck (Γ_1). Note that Λ is a positive dimensionless constant independent of any parameters (including W); our boundary-element calculations in an infinite square channel provide a value of $\Lambda \approx 0.17$.

As the bacterium swims through the channel, the torque dipole resulting from the counter-rotation of the cell body and flagella produces a net torque on the puck:

$$\Gamma \hat{\mathbf{z}} = \Gamma_1 \hat{\mathbf{z}} + \Gamma_2 \hat{\mathbf{z}} = -\Lambda \frac{\ell_D}{W} \Gamma_M \hat{\mathbf{z}}, \quad (6)$$

where $\ell_D = x_1 - x_2$ is the dipole length. Notably, the torque magnitude Γ is independent of the position of the bacterium under the puck, provided that both rotlets are inside the channel; it is also independent of the orientation of the bacterium ($+\hat{\mathbf{x}}$ or $-\hat{\mathbf{x}}$) along the channel axis, as observed in the experiment (Supplementary Fig. 6).

We can now describe the angular dynamics of the puck. We denote by $X_B(t) = U_s t$ the instantaneous position of the bacterium inside the channel, measured from the channel entrance. Here, U_s , the bacterial swim speed, is constant, as measured experimentally (Fig. 2a). If both rotlets are contained inside the channel, the torque

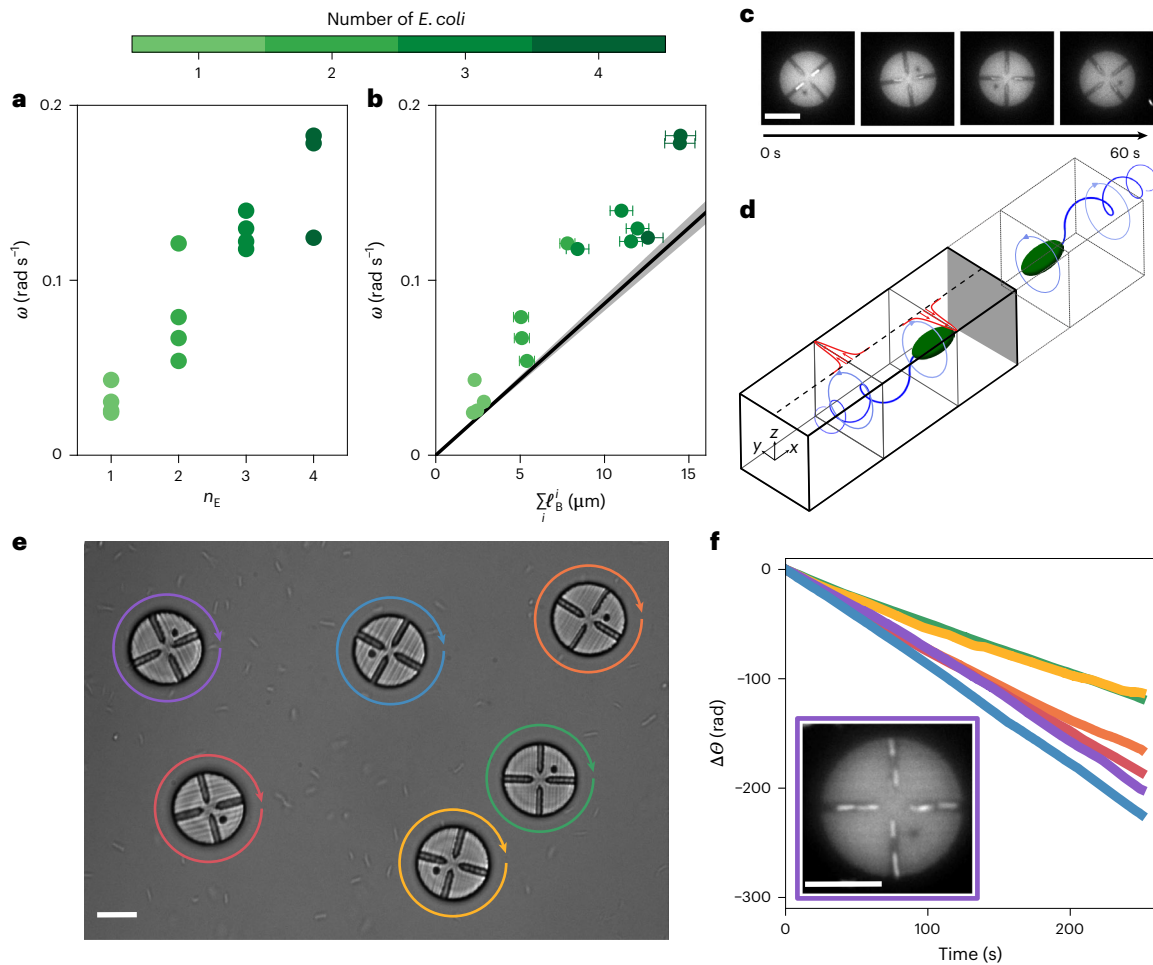


Fig. 4 | Dynamics of pucks with chambers. **a**, Rotation rates ω for pucks with chambers, as seen in Fig. 1d, for different occupancy levels n_E of the bacteria in the chambers. For all occupancy numbers ($n_E > 0$), the pucks rotate clockwise, with ω increasing with the number of bacteria in the chambers. This highlights the cumulative effect of the entrainment mechanism. **b**, The data from **a** ($\omega(n_E)$) collapse when ω is plotted as a function of the total body length inside the channels ($\sum_i \ell_B^i$), as predicted by the model. The black line indicates the prediction from the hydrodynamic model, which accounts for the hydrodynamics of a closed chamber rather than an infinite channel, as visible in **d**. Data symbols with error bars are centred on the value (ω) from **a** with a standard deviation from the determination of the bacterial length (ℓ_B) using

fluorescence microscopy. **c**, Time-lapse fluorescence microscopy images of a puck with one *E. coli* bacterium trapped inside each chamber. **d**, Schematic of the hydrodynamic model for the closed chamber, instead of the infinite channel in Fig. 3. The no-slip condition at the end of the chamber is implemented by placing an image system symmetrically on the other side of the wall. **e**, Experiment with six pucks with chambers suspended in a bath of motile *E. coli*. All pucks spin clockwise, marking a first step towards the development of chiral fluids of spinners. **f**, Dynamics $\Delta\theta(t)$ for each puck from **e**. The pucks rotated persistently for minutes at speeds up to 10 rpm. Inset: fluorescence microscopy image of a puck with four closed channels, each accommodating several *E. coli*, which rotated faster. Scale bars, 10 μm .

on the puck is constant and given by equation (6), resulting in the angular velocity:

$$\frac{d\theta}{dt} = M_\theta \Gamma, \tag{7}$$

where M_θ is the rotational mobility of the puck for rotation around the z axis. The value of M_θ is obtained from the Stokes–Einstein relation, $M_\theta = D_\theta/k_B T$, where k_B is the Boltzmann constant and T is temperature. The rotational diffusivity of the puck in a thermal bath was measured independently: $D_\theta = (6 \pm 1) \times 10^{-5} \text{ rad}^2 \text{ s}^{-1}$ (Supplementary Fig. 4). Integrating equation (7) and eliminating time using the swim speed provides the angular displacement as a function of the position X_B of the bacterium in the channel:

$$\Delta\theta(X_B) = -\Lambda \frac{\ell_D}{W} \frac{M_\theta}{U_s} \Gamma_M X_B. \tag{8}$$

This relation predicts clockwise rotation of the puck and captures the linear decrease observed in the experimental data (Fig. 2c,g). All the prefactors in equation (8) can be estimated based on experiments (Supplementary Table 1), with the exception of the dipole length ℓ_D . The collapse of the angular displacements upon scaling $\Delta\theta$ with cell body length in Fig. 2f points at a linear relation between ℓ_D and ℓ_B , and therefore, we posit that $\ell_D = \alpha \ell_B$. The dimensionless parameter α is the only fitting parameter in our model. By fitting equation (8) to the experimental data, we estimate $\alpha \approx 1.5$.

This simple hydrodynamic model allows us to explain the anti-clockwise rotation of the puck, as observed in the second half of the down–up shape (Fig. 2c,g). As the cell body exits the channel, it ceases to exert a torque on the puck, which is now only subject to the torque Γ_2 due to the rotating flagella, thus causing a change in the direction of rotation. We estimate the angular displacement beyond that point to be

$$\Delta\theta(X_B) = \frac{\Lambda}{W} \frac{M_\theta}{U_s} \Gamma_M \left[\frac{X_B^2}{2} + X_B(\ell_B - \ell_D - R) + \frac{\ell_B(\ell_B - 2R)}{2} \right], \tag{9}$$

which predicts a reversal in the direction of rotation with a quadratic dependence on position. The hydrodynamic model provides a quantitative description of the rotation through equations (8) and (9). The rotation is controlled by either the two rotlets or a single one inside the channel. The transition is observed in the experiment as the position of reversal of the down–up shape (Fig. 2c).

Discussion

We now inspect the physical implications of this hydrodynamic mechanism. First, the entrainment of the puck by a torque dipole explains the characteristic down–up shape observed in the experiment: when both rotlets are inside the channel, the puck rotates clockwise, and the direction of rotation reverses when a single rotlet remains in the channel. In effect, the model quantitatively reproduces our experimental findings (Fig. 3c) by capturing both the reversal of the direction of rotation and the depths $\Delta\theta_{\max}$ observed in the experiment. In the experiment, the minimum, corresponding to the reversal of the direction of rotation of the puck, is observed near $X_B \approx 2R - \ell_B$ (Fig. 2d). Naively, we expected the reversal of direction and position of the minimum to occur at $X_B = 2R$ when the centre of the body of the *E. coli* exits the channel. We highlight two important simplifications in our far-field model that could explain this discrepancy and will require further work. First, the flagella form a deformable bundle of proteins whose complex dynamics are not fully captured by the point rotlet hydrodynamic description and may be affected by the geometric confinement. Second, we considered infinite channels in the model, whereas a near-field description might be required to fully describe the experimental results, especially at the point where the *E. coli* exits the channel. Nonetheless, the experimental observations confirm our intuition that the dipole length is linearly dependent on the size of the bacterium body $\ell_D = \alpha\ell_B$, with $\alpha = O(1)$, and our experiments are well captured by the model with a single parameter $\alpha = 1.5$.

We now return to our experimental observations of pucks with chambers (Fig. 1d) in light of our mechanistic understanding. The hydrodynamic model presented in the section ‘Hydrodynamic model’ shows that when both the body and flagella of the *E. coli* are confined beneath the puck, they exert a torque on the puck, leading to persistent clockwise rotation. This torque always rotates the puck clockwise, regardless of the precise orientation of the cell inside the chamber; this explains the behaviour previously reported, whereby the puck rotates faster as other chambers are filled (Fig. 1f). Guided by our hydrodynamic model, we realized that the total length of trapped bacteria, rather than their number, should set the rotation rate, and we collapsed the observed rotation rates of the puck $\omega \propto \sum_i \ell_B^i$, where ℓ_B^i is the measured length of the body of bacterium *i* in the chamber (Fig. 4a,b). Furthermore, by simply modifying the hydrodynamics of an open channel to a closed one, our hydrodynamic model accurately predicts the observed rotation speeds (Fig. 4d). The clockwise rotation persists over the course of minutes at speeds comparable with asymmetric ratchets in bacterial baths^{9,10}. This provides a way to form chiral fluids of spinners made of hybrid *E. coli*, micromachines that persistently rotate in the absence of geometric asymmetry. As a first step in this direction, we show a collection of discs powered by a bacterial bath (Fig. 4e and Supplementary Video 4). The rotation could be tuned by modifying the number of channels. The spinners can be fabricated with commercially available two-photon-polymerization nanoprinters. Notably, our experimental results highlight that capturing several bacteria inside narrow chambers (Fig. 4f inset) increases the rotation rate up to 10 rpm (Fig. 4f), which again demonstrates the salient role of confinement in enhancing the hydrodynamic effect.

Conclusion

We unveiled a new mechanism for transducing the mechanical work of rotating flagellar nanomotors into the rotation of symmetric objects. The mechanism bridges orders of magnitude of scales, as

confinement couples to the hydrodynamic torque dipole of swimming *E. coli* to power objects adjacent to the bacteria. Beyond the conceptual advance, our findings show powerful differences in comparison with the mechanism of rotation of asymmetric gears by rectification of flagellar thrust, as previously reported, for example, in refs. 9,10,12. Because the rotation emerges from confinement and the chirality of the BFM, it is agnostic to the shape of the object or the careful positioning of the bacteria underneath it. In practice, our results show that the torque dipole of organisms with rotary flagella should be important in a broad range of confinement situations, whether in natural, ecological or artificial settings. In light of the success of applying the force dipole to the description of biological systems and active matter^{27–31}, the fluid mechanics implications of our findings remain to be explored. Our findings highlight the interplay between bacterial navigation and their environments, which has potential ecological implications, and they also reveal a new mechanism for assembling unconventional gels in bacterial baths²⁰. Finally, our results provide a way to characterize aspects of individual bacterial physiology, such as the distribution of BFM torque in a population or its dependence on the chemical environment, as well as other properties of biological relevance.

Online content

Any methods, additional references, Nature Portfolio reporting summaries, source data, extended data, supplementary information, acknowledgements, peer review information; details of author contributions and competing interests; and statements of data and code availability are available at <https://doi.org/10.1038/s41567-026-03189-4>.

References

- Purcell, E. M. Life at low Reynolds number. *Am. J. Phys.* **45**, 3–11 (1977).
- Manson, M. D., Tedesco, P., Berg, H. C., Harold, F. M. & Drift, C. V. D. A protonmotive force drives bacterial flagella. *Proc. Natl Acad. Sci. USA* **74**, 3060–3064 (1977).
- Berg, H. C. & Brown, D. A. Chemotaxis in *Escherichia coli* analysed by three-dimensional tracking. *Nature* **239**, 500–504 (1972).
- Berg, H. C. Motile behavior of bacteria. *Phys. Today* **53**, 24–29 (2000).
- Wu, X.-L. & Libchaber, A. Particle diffusion in a quasi-two-dimensional bacterial bath. *Phys. Rev. Lett.* **84**, 3017–3020 (2000).
- Leptos, K. C., Guasto, J. S., Gollub, J. P., Pesci, A. I. & Goldstein, R. E. Dynamics of enhanced tracer diffusion in suspensions of swimming eukaryotic microorganisms. *Phys. Rev. Lett.* **103**, 198103 (2009).
- Miño, G. et al. Enhanced diffusion due to active swimmers at a solid surface. *Phys. Rev. Lett.* **106**, 048102 (2011).
- Jepson, A., Martinez, V. A., Schwarz-Linek, J., Morozov, A. & Poon, W. C. K. Enhanced diffusion of nonswimmers in a three-dimensional bath of motile bacteria. *Phys. Rev. E* **88**, 041002 (2013).
- Leonardo, R. D. et al. Bacterial ratchet motors. *Proc. Natl Acad. Sci. USA* **107**, 9541–9545 (2010).
- Sokolov, A., Apodaca, M. M., Grzybowski, B. A. & Aranson, I. S. Swimming bacteria power microscopic gears. *Proc. Natl Acad. Sci. USA* **107**, 969–974 (2010).
- Angelani, L., Di Leonardo, R. & Ruocco, G. Self-starting micromotors in a bacterial bath. *Phys. Rev. Lett.* **102**, 048104 (2009).
- Viznyiczai, G. et al. Light controlled 3D micromotors powered by bacteria. *Nat. Commun.* **8**, 15974 (2017).
- Maggi, C. et al. Self-assembly of micromachining systems powered by Janus micromotors. *Small* **12**, 446–451 (2016).
- Pellicciotta, N., Bagal, O. S., Cannarsa, M. C., Bianchi, S. & Di Leonardo, R. Wall torque controls propulsion of curved microstructures in bacterial baths. *Phys. Rev. Lett.* **135**, 138302 (2025).
- Koumakis, N., Lepore, A., Maggi, C. & Leonardo, R. D. Targeted delivery of colloids by swimming bacteria. *Nat. Commun.* **4**, 2588 (2013).

16. Steager, E. B. et al. Electrokinetic and optical control of bacterial microrobots. *J. Micromech. Microeng* **21**, 035001 (2011).
17. Carlsen, R. W., Edwards, M. R., Zhuang, J., Pacoret, C. & Sitti, M. Magnetic steering control of multi-cellular bio-hybrid microswimmers. *Lab Chip* **14**, 3850–3859 (2014).
18. Hiratsuka, Y., Miyata, M., Tada, T. & Uyeda, T. Q. P. A microrotary motor powered by bacteria. *Proc. Natl Acad. Sci. USA* **103**, 13618–13623 (2006).
19. Di Leonardo, R., Dell’Arciprete, D., Angelani, L. & Iebba, V. Swimming with an image. *Phys. Rev. Lett.* **106**, 038101 (2011).
20. Grober, D. et al. Unconventional colloidal aggregation in chiral bacterial baths. *Nat. Phys.* **19**, 1680–1688 (2023).
21. Drescher, K., Dunkel, J., Cisneros, L. H., Ganguly, S. & Goldstein, R. E. Fluid dynamics and noise in bacterial cell-cell and cell-surface scattering. *Proc. Natl Acad. Sci. USA* **108**, 10940–10945 (2011).
22. Berke, A. P., Turner, L., Berg, H. C. & Lauga, E. Hydrodynamic attraction of swimming microorganisms by surfaces. *Phys. Rev. Lett.* **101**, 038102 (2008).
23. Lauga, E., DiLuzio, W. R., Whitesides, G. M. & Stone, H. A. Swimming in circles: motion of bacteria near solid boundaries. *Biophys. J.* **90**, 400–412 (2006).
24. Chattopadhyay, S., Moldovan, R., Yeung, C. & Wu, X. L. Swimming efficiency of bacterium *Escherichia coli*. *Proc. Natl Acad. Sci. USA* **103**, 13712–13717 (2006).
25. Turner, L., Stern, A. S. & Berg, H. C. Growth of flagellar filaments of *Escherichia coli* is independent of filament length. *J. Bacteriol.* **194**, 2437–2442 (2012).
26. Pozrikidis, C. in *Boundary Integral and Singularity Methods for Linearized Viscous Flow* Ch. 2 and 6 (Cambridge Univ. Press, 1992); <https://doi.org/10.1017/CBO9780511624124>.
27. Saintillan, D. Rheology of active fluids. *Annu. Rev. Fluid Mech.* **50**, 563–592 (2018).
28. Simha, R. A. & Ramaswamy, S. Hydrodynamic fluctuations and instabilities in ordered suspensions of self-propelled particles. *Phys. Rev. Lett.* **89**, 058101 (2002).
29. Marchetti, M. C. et al. Hydrodynamics of soft active matter. *Rev. Mod. Phys.* **85**, 1143–1189 (2013).
30. López, H. M., Gachelin, J., Douarche, C., Auradou, H. & Clément, E. Turning bacteria suspensions into superfluids. *Phys. Rev. Lett.* **115**, 028301 (2015).
31. Doostmohammadi, A., Ignés-Mullol, J., Yeomans, J. M. & Sagués, F. Active nematics. *Nat. Commun.* **9**, 3246 (2018).

Publisher’s note Springer Nature remains neutral with regard to jurisdictional claims in published maps and institutional affiliations.

Open Access This article is licensed under a Creative Commons Attribution 4.0 International License, which permits use, sharing, adaptation, distribution and reproduction in any medium or format, as long as you give appropriate credit to the original author(s) and the source, provide a link to the Creative Commons licence, and indicate if changes were made. The images or other third party material in this article are included in the article’s Creative Commons licence, unless indicated otherwise in a credit line to the material. If material is not included in the article’s Creative Commons licence and your intended use is not permitted by statutory regulation or exceeds the permitted use, you will need to obtain permission directly from the copyright holder. To view a copy of this licence, visit <http://creativecommons.org/licenses/by/4.0/>.

© The Author(s) 2026

Methods

Stock solutions

For all stock solutions, chemicals were dissolved in deionized (DI) water with a resistivity of 18 M Ω cm from a water purification system (Milli-Q EQ 7000). A stock solution of 5% w/v F 108 (Sigma-Aldrich Synperonic F 108 surfactant, molecular weight (MW) of 14,600) was prepared by dissolving 50 g of F 108 in 1 l of DI water. A stock solution of 0.1 M potassium phosphate buffer (pH 8), which was used to prepare the motility medium, was prepared by dissolving 16.28 g of K₂HPO₄ (Sigma-Aldrich, MW 174.2) and 0.887 g of KH₂PO₄ (Sigma-Aldrich, MW 136.1) in 1 l of DI water. Finally, 0.5 M of ethylenediaminetetraacetic acid (EDTA) stock solution was prepared by dissolving 186.10 g of EDTA dihydrate (Sigma-Aldrich, MW 372.2) into 1 l of DI water. To dissolve the EDTA, the pH was adjusted to 8 using NaOH pellets. A stock solution of sterile ampicillin 100 mg ml⁻¹ was purchased from Sigma-Aldrich. A 1 M L-serine solution was made by dissolving 1.05 g of L-serine powder (Sigma-Aldrich, MW 105.09 g mol⁻¹) into 10 ml of DI water.

E. coli growth

E. coli (strain MG1655) were labelled with GFP by in-house transformation using a standard electroporation protocol and a DNA plasmid containing both the GFP gene and an ampicillin-resistance gene.

Cultures were grown from single colonies on agar plates containing 100 μ g ml⁻¹ ampicillin. Cultures were grown overnight until saturation at 33 °C while being shaken at 200 rpm and in tryptone broth containing 10 g l⁻¹ tryptone, and 5 g l⁻¹ NaCl. The saturated culture was diluted 1:100 with fresh tryptone broth and grown at 33 °C until the optical density was 0.5, corresponding to the mid-exponential growth phase. Then, 1 ml of cells was centrifuged at 330g for 10 min until a pellet formed.

Cells were washed and gently resuspended in motility medium containing 1 mM potassium phosphate buffer (pH 8) and 0.1 mM EDTA (pH 8). This process was performed three times to ensure that the growth media had been sufficiently removed. In the final step, the optical density was remeasured and the final volume of motility medium was adjusted, yielding a concentrated sample of motile *E. coli* at an optical density of 1.

Preparation of custom 3D-printed pucks

The 3D-printed pucks were printed using a commercial high-resolution two-photon-polymerization 3D-printing system (NanoOne, UpNano). The pucks were designed using OnShape CAD software. Glass coverslips (No. 1.5H high precision, 170 \pm 5 μ m, Zeiss) were cleaned via 10-min sonication in 1% Hellmanex solution, followed by 10-min sonication in DI water and finally by plasma-cleaning for 10 min. A 50 \times 50 array of pucks was printed directly onto a glass coverslip ('bottom-up' printing mode) using a \times 40 objective (numerical aperture 1.4 and working distance 130 μ m) and UpBrix printing resin and applying standard fine-resolution printing parameters. Leftover resin was cleaned off with a 10-min soak in PGMEA solution ((1-methyl-2-propyl) acetate, Sigma-Aldrich), followed by a 2-min soak in 2-propanol (99.5% pure, Sigma-Aldrich).

Finally, the pucks were transferred to a 50-ml Falcon tube containing 5% F 108 stock solution and sonicated for 10 min to detach them from the glass coverslip. The coverslip was subsequently removed, and the pucks were allowed to sediment to the bottom. Finally, 1 ml was pipetted from the bottom of the tube, yielding a concentrated suspension of pucks dispersed in 5% F 108 surfactant. This process is illustrated in Supplementary Fig. 1.

Pucks in solution

The concentrated solution of *E. coli* suspended in motility media was first diluted to the desired concentration, up to a maximum of $\rho = 6 \times 10^8$ cells per millilitre. L-serine stock solution (1 M) was added

to enhance *E. coli* motility to a final concentration of 50 mM. Finally, pucks suspended in 5% F 108 surfactant were added to a final concentration of 0.25% F 108. The solution was confined in a 3 mm \times 0.3 mm \times 50 mm rectangular glass capillary and placed on a glass slide sealed with a wax pen. The glass capillary had previously been cleaned by sonication in 1% Hellmanex solution and washed by sonication in DI water.

Reporting summary

Further information on research design is available in the Nature Portfolio Reporting Summary linked to this article.

Data availability

The datasets generated and analysed during the current study are openly available via Zenodo at <https://doi.org/10.5281/zenodo.15236674> (ref. 32). All data are released under the CC-BY 4.0 licence. For any further questions about data access or reuse, please contact the corresponding author.

References

- Grober, D., Dhar, T., Saintillan, D. & Palacci, J. Supporting data for 'The hydrodynamic torque dipole from rotary bacterial flagella powers symmetric discs'. Zenodo <https://doi.org/10.5281/zenodo.15236674> (2025).

Acknowledgements

We thank E. Krasnopeeva for help with the bacterial culture, motility and genetic engineering. We thank Q. Martinet for help with the experimental design, F. Pertl for atomic force microscopy measurements and S. Hajek for the scanning electron microscopy imaging. This project has received funding from the European Research Council under the European Union's Horizon Europe research and innovation programme (VULCAN, 101086998). The views and opinions expressed are, however, those of the authors only and do not necessarily reflect those of the European Union or the European Research Council Executive Agency. Neither the European Union nor the granting authority can be held responsible for them. J.P. thanks the Nanofabrication and Electron Microscopy Shared Scientific Units of ISTA for support.

Author contributions

D.G. and J.P. conceived the experiment. D.G. performed and analysed the experiments. T.D. and D.S. developed and analysed the model. All authors wrote, reviewed and commented on the paper.

Funding

Open access funding provided by Institute of Science and Technology (IST Austria).

Competing interests

The authors declare no competing interests.

Additional information

Supplementary information The online version contains supplementary material available at <https://doi.org/10.1038/s41567-026-03189-4>.

Correspondence and requests for materials should be addressed to Jérémie Palacci.

Peer review information *Nature Physics* thanks the anonymous reviewers for their contribution to the peer review of this work.

Reprints and permissions information is available at www.nature.com/reprints.

Reporting Summary

Nature Portfolio wishes to improve the reproducibility of the work that we publish. This form provides structure for consistency and transparency in reporting. For further information on Nature Portfolio policies, see our [Editorial Policies](#) and the [Editorial Policy Checklist](#).

Statistics

For all statistical analyses, confirm that the following items are present in the figure legend, table legend, main text, or Methods section.

n/a | Confirmed

- The exact sample size (n) for each experimental group/condition, given as a discrete number and unit of measurement
- A statement on whether measurements were taken from distinct samples or whether the same sample was measured repeatedly
- The statistical test(s) used AND whether they are one- or two-sided
Only common tests should be described solely by name; describe more complex techniques in the Methods section.
- A description of all covariates tested
- A description of any assumptions or corrections, such as tests of normality and adjustment for multiple comparisons
- A full description of the statistical parameters including central tendency (e.g. means) or other basic estimates (e.g. regression coefficient) AND variation (e.g. standard deviation) or associated estimates of uncertainty (e.g. confidence intervals)
- For null hypothesis testing, the test statistic (e.g. F , t , r) with confidence intervals, effect sizes, degrees of freedom and P value noted
Give P values as exact values whenever suitable.
- For Bayesian analysis, information on the choice of priors and Markov chain Monte Carlo settings
- For hierarchical and complex designs, identification of the appropriate level for tests and full reporting of outcomes
- Estimates of effect sizes (e.g. Cohen's d , Pearson's r), indicating how they were calculated

Our web collection on [statistics for biologists](#) contains articles on many of the points above.

Software and code

Policy information about [availability of computer code](#)

Data collection

Provide a description of all commercial, open source and custom code used to collect the data in this study, specifying the version used OR state that no software was used.

Data analysis

The datasets generated and/or analyzed during the current study are openly available in the Zenodo repository, at <https://doi.org/10.5281/zenodo.15236674>. All data are released under the CC-BY 4.0 license. For any further questions about data access or reuse, please contact the corresponding author.

For manuscripts utilizing custom algorithms or software that are central to the research but not yet described in published literature, software must be made available to editors and reviewers. We strongly encourage code deposition in a community repository (e.g. GitHub). See the Nature Portfolio [guidelines for submitting code & software](#) for further information.

Data

Policy information about [availability of data](#)

All manuscripts must include a [data availability statement](#). This statement should provide the following information, where applicable:

- Accession codes, unique identifiers, or web links for publicly available datasets
- A description of any restrictions on data availability
- For clinical datasets or third party data, please ensure that the statement adheres to our [policy](#)

The datasets generated and/or analyzed during the current study are openly available in the Zenodo repository, at <https://doi.org/10.5281/zenodo.15236674>. All data are released under the CC-BY 4.0 license. For any further questions about data access or reuse, please contact the corresponding author.

Research involving human participants, their data, or biological material

Policy information about studies with [human participants or human data](#). See also policy information about [sex, gender \(identity/presentation\), and sexual orientation](#) and [race, ethnicity and racism](#).

Reporting on sex and gender

Use the terms sex (biological attribute) and gender (shaped by social and cultural circumstances) carefully in order to avoid confusing both terms. Indicate if findings apply to only one sex or gender; describe whether sex and gender were considered in study design; whether sex and/or gender was determined based on self-reporting or assigned and methods used. Provide in the source data disaggregated sex and gender data, where this information has been collected, and if consent has been obtained for sharing of individual-level data; provide overall numbers in this Reporting Summary. Please state if this information has not been collected. Report sex- and gender-based analyses where performed, justify reasons for lack of sex- and gender-based analysis.

Reporting on race, ethnicity, or other socially relevant groupings

Please specify the socially constructed or socially relevant categorization variable(s) used in your manuscript and explain why they were used. Please note that such variables should not be used as proxies for other socially constructed/relevant variables (for example, race or ethnicity should not be used as a proxy for socioeconomic status). Provide clear definitions of the relevant terms used, how they were provided (by the participants/respondents, the researchers, or third parties), and the method(s) used to classify people into the different categories (e.g. self-report, census or administrative data, social media data, etc.) Please provide details about how you controlled for confounding variables in your analyses.

Population characteristics

Describe the covariate-relevant population characteristics of the human research participants (e.g. age, genotypic information, past and current diagnosis and treatment categories). If you filled out the behavioural & social sciences study design questions and have nothing to add here, write "See above."

Recruitment

Describe how participants were recruited. Outline any potential self-selection bias or other biases that may be present and how these are likely to impact results.

Ethics oversight

Identify the organization(s) that approved the study protocol.

Note that full information on the approval of the study protocol must also be provided in the manuscript.

Field-specific reporting

Please select the one below that is the best fit for your research. If you are not sure, read the appropriate sections before making your selection.

Life sciences Behavioural & social sciences Ecological, evolutionary & environmental sciences

For a reference copy of the document with all sections, see [nature.com/documents/nr-reporting-summary-flat.pdf](https://www.nature.com/documents/nr-reporting-summary-flat.pdf)

Life sciences study design

All studies must disclose on these points even when the disclosure is negative.

Sample size

Describe how sample size was determined, detailing any statistical methods used to predetermine sample size OR if no sample-size calculation was performed, describe how sample sizes were chosen and provide a rationale for why these sample sizes are sufficient.

Data exclusions

Describe any data exclusions. If no data were excluded from the analyses, state so OR if data were excluded, describe the exclusions and the rationale behind them, indicating whether exclusion criteria were pre-established.

Replication

Describe the measures taken to verify the reproducibility of the experimental findings. If all attempts at replication were successful, confirm this OR if there are any findings that were not replicated or cannot be reproduced, note this and describe why.

Randomization

Describe how samples/organisms/participants were allocated into experimental groups. If allocation was not random, describe how covariates were controlled OR if this is not relevant to your study, explain why.

Blinding

Describe whether the investigators were blinded to group allocation during data collection and/or analysis. If blinding was not possible,

Behavioural & social sciences study design

All studies must disclose on these points even when the disclosure is negative.

Study description	<i>Briefly describe the study type including whether data are quantitative, qualitative, or mixed-methods (e.g. qualitative cross-sectional, quantitative experimental, mixed-methods case study).</i>
Research sample	<i>State the research sample (e.g. Harvard university undergraduates, villagers in rural India) and provide relevant demographic information (e.g. age, sex) and indicate whether the sample is representative. Provide a rationale for the study sample chosen. For studies involving existing datasets, please describe the dataset and source.</i>
Sampling strategy	<i>Describe the sampling procedure (e.g. random, snowball, stratified, convenience). Describe the statistical methods that were used to predetermine sample size OR if no sample-size calculation was performed, describe how sample sizes were chosen and provide a rationale for why these sample sizes are sufficient. For qualitative data, please indicate whether data saturation was considered, and what criteria were used to decide that no further sampling was needed.</i>
Data collection	<i>Provide details about the data collection procedure, including the instruments or devices used to record the data (e.g. pen and paper, computer, eye tracker, video or audio equipment) whether anyone was present besides the participant(s) and the researcher, and whether the researcher was blind to experimental condition and/or the study hypothesis during data collection.</i>
Timing	<i>Indicate the start and stop dates of data collection. If there is a gap between collection periods, state the dates for each sample cohort.</i>
Data exclusions	<i>If no data were excluded from the analyses, state so OR if data were excluded, provide the exact number of exclusions and the rationale behind them, indicating whether exclusion criteria were pre-established.</i>
Non-participation	<i>State how many participants dropped out/declined participation and the reason(s) given OR provide response rate OR state that no participants dropped out/declined participation.</i>
Randomization	<i>If participants were not allocated into experimental groups, state so OR describe how participants were allocated to groups, and if allocation was not random, describe how covariates were controlled.</i>

Ecological, evolutionary & environmental sciences study design

All studies must disclose on these points even when the disclosure is negative.

Study description	<i>Briefly describe the study. For quantitative data include treatment factors and interactions, design structure (e.g. factorial, nested, hierarchical), nature and number of experimental units and replicates.</i>
Research sample	<i>Describe the research sample (e.g. a group of tagged <i>Passer domesticus</i>, all <i>Stenocereus thurberi</i> within Organ Pipe Cactus National Monument), and provide a rationale for the sample choice. When relevant, describe the organism taxa, source, sex, age range and any manipulations. State what population the sample is meant to represent when applicable. For studies involving existing datasets, describe the data and its source.</i>
Sampling strategy	<i>Note the sampling procedure. Describe the statistical methods that were used to predetermine sample size OR if no sample-size calculation was performed, describe how sample sizes were chosen and provide a rationale for why these sample sizes are sufficient.</i>
Data collection	<i>Describe the data collection procedure, including who recorded the data and how.</i>
Timing and spatial scale	<i>Indicate the start and stop dates of data collection, noting the frequency and periodicity of sampling and providing a rationale for these choices. If there is a gap between collection periods, state the dates for each sample cohort. Specify the spatial scale from which the data are taken</i>
Data exclusions	<i>If no data were excluded from the analyses, state so OR if data were excluded, describe the exclusions and the rationale behind them, indicating whether exclusion criteria were pre-established.</i>
Reproducibility	<i>Describe the measures taken to verify the reproducibility of experimental findings. For each experiment, note whether any attempts to repeat the experiment failed OR state that all attempts to repeat the experiment were successful.</i>
Randomization	<i>Describe how samples/organisms/participants were allocated into groups. If allocation was not random, describe how covariates were controlled. If this is not relevant to your study, explain why.</i>
Blinding	<i>Describe the extent of blinding used during data acquisition and analysis. If blinding was not possible, describe why OR explain why blinding was not relevant to your study.</i>

Did the study involve field work? Yes No

Field work, collection and transport

Field conditions	<i>Describe the study conditions for field work, providing relevant parameters (e.g. temperature, rainfall).</i>
Location	<i>State the location of the sampling or experiment, providing relevant parameters (e.g. latitude and longitude, elevation, water depth).</i>
Access & import/export	<i>Describe the efforts you have made to access habitats and to collect and import/export your samples in a responsible manner and in compliance with local, national and international laws, noting any permits that were obtained (give the name of the issuing authority, the date of issue, and any identifying information).</i>
Disturbance	<i>Describe any disturbance caused by the study and how it was minimized.</i>

Reporting for specific materials, systems and methods

We require information from authors about some types of materials, experimental systems and methods used in many studies. Here, indicate whether each material, system or method listed is relevant to your study. If you are not sure if a list item applies to your research, read the appropriate section before selecting a response.

Materials & experimental systems

n/a	Involvement in the study
<input type="checkbox"/>	<input type="checkbox"/> Antibodies
<input type="checkbox"/>	<input type="checkbox"/> Eukaryotic cell lines
<input type="checkbox"/>	<input type="checkbox"/> Palaeontology and archaeology
<input type="checkbox"/>	<input type="checkbox"/> Animals and other organisms
<input type="checkbox"/>	<input type="checkbox"/> Clinical data
<input type="checkbox"/>	<input type="checkbox"/> Dual use research of concern
<input type="checkbox"/>	<input type="checkbox"/> Plants

Methods

n/a	Involvement in the study
<input type="checkbox"/>	<input type="checkbox"/> ChIP-seq
<input type="checkbox"/>	<input type="checkbox"/> Flow cytometry
<input type="checkbox"/>	<input type="checkbox"/> MRI-based neuroimaging

Antibodies

Antibodies used	<i>Describe all antibodies used in the study; as applicable, provide supplier name, catalog number, clone name, and lot number.</i>
Validation	<i>Describe the validation of each primary antibody for the species and application, noting any validation statements on the manufacturer's website, relevant citations, antibody profiles in online databases, or data provided in the manuscript.</i>

Eukaryotic cell lines

Policy information about [cell lines and Sex and Gender in Research](#)

Cell line source(s)	<i>State the source of each cell line used and the sex of all primary cell lines and cells derived from human participants or vertebrate models.</i>
Authentication	<i>Describe the authentication procedures for each cell line used OR declare that none of the cell lines used were authenticated.</i>
Mycoplasma contamination	<i>Confirm that all cell lines tested negative for mycoplasma contamination OR describe the results of the testing for mycoplasma contamination OR declare that the cell lines were not tested for mycoplasma contamination.</i>
Commonly misidentified lines (See ICLAC register)	<i>Name any commonly misidentified cell lines used in the study and provide a rationale for their use.</i>

Palaeontology and Archaeology

Specimen provenance	<i>Provide provenance information for specimens and describe permits that were obtained for the work (including the name of the issuing authority, the date of issue, and any identifying information). Permits should encompass collection and, where applicable, export.</i>
Specimen deposition	<i>Indicate where the specimens have been deposited to permit free access by other researchers.</i>

Dating methods

If new dates are provided, describe how they were obtained (e.g. collection, storage, sample pretreatment and measurement), where they were obtained (i.e. lab name), the calibration program and the protocol for quality assurance OR state that no new dates are provided.

Tick this box to confirm that the raw and calibrated dates are available in the paper or in Supplementary Information.

Ethics oversight

Identify the organization(s) that approved or provided guidance on the study protocol, OR state that no ethical approval or guidance was required and explain why not.

Note that full information on the approval of the study protocol must also be provided in the manuscript.

Animals and other research organisms

Policy information about [studies involving animals](#); [ARRIVE guidelines](#) recommended for reporting animal research, and [Sex and Gender in Research](#)

Laboratory animals

For laboratory animals, report species, strain and age OR state that the study did not involve laboratory animals.

Wild animals

Provide details on animals observed in or captured in the field; report species and age where possible. Describe how animals were caught and transported and what happened to captive animals after the study (if killed, explain why and describe method; if released, say where and when) OR state that the study did not involve wild animals.

Reporting on sex

Indicate if findings apply to only one sex; describe whether sex was considered in study design, methods used for assigning sex. Provide data disaggregated for sex where this information has been collected in the source data as appropriate; provide overall numbers in this Reporting Summary. Please state if this information has not been collected. Report sex-based analyses where performed, justify reasons for lack of sex-based analysis.

Field-collected samples

For laboratory work with field-collected samples, describe all relevant parameters such as housing, maintenance, temperature, photoperiod and end-of-experiment protocol OR state that the study did not involve samples collected from the field.

Ethics oversight

Identify the organization(s) that approved or provided guidance on the study protocol, OR state that no ethical approval or guidance was required and explain why not.

Note that full information on the approval of the study protocol must also be provided in the manuscript.

Clinical data

Policy information about [clinical studies](#)

All manuscripts should comply with the ICMJE [guidelines for publication of clinical research](#) and a completed [CONSORT checklist](#) must be included with all submissions.

Clinical trial registration

Provide the trial registration number from ClinicalTrials.gov or an equivalent agency.

Study protocol

Note where the full trial protocol can be accessed OR if not available, explain why.

Data collection

Describe the settings and locales of data collection, noting the time periods of recruitment and data collection.

Outcomes

Describe how you pre-defined primary and secondary outcome measures and how you assessed these measures.

Dual use research of concern

Policy information about [dual use research of concern](#)

Hazards

Could the accidental, deliberate or reckless misuse of agents or technologies generated in the work, or the application of information presented in the manuscript, pose a threat to:

- | No | Yes | |
|--------------------------|--------------------------|----------------------------|
| <input type="checkbox"/> | <input type="checkbox"/> | Public health |
| <input type="checkbox"/> | <input type="checkbox"/> | National security |
| <input type="checkbox"/> | <input type="checkbox"/> | Crops and/or livestock |
| <input type="checkbox"/> | <input type="checkbox"/> | Ecosystems |
| <input type="checkbox"/> | <input type="checkbox"/> | Any other significant area |

Experiments of concern

Does the work involve any of these experiments of concern:

- | No | Yes | |
|--------------------------|--------------------------|---|
| <input type="checkbox"/> | <input type="checkbox"/> | Demonstrate how to render a vaccine ineffective |
| <input type="checkbox"/> | <input type="checkbox"/> | Confer resistance to therapeutically useful antibiotics or antiviral agents |
| <input type="checkbox"/> | <input type="checkbox"/> | Enhance the virulence of a pathogen or render a nonpathogen virulent |
| <input type="checkbox"/> | <input type="checkbox"/> | Increase transmissibility of a pathogen |
| <input type="checkbox"/> | <input type="checkbox"/> | Alter the host range of a pathogen |
| <input type="checkbox"/> | <input type="checkbox"/> | Enable evasion of diagnostic/detection modalities |
| <input type="checkbox"/> | <input type="checkbox"/> | Enable the weaponization of a biological agent or toxin |
| <input type="checkbox"/> | <input type="checkbox"/> | Any other potentially harmful combination of experiments and agents |

Plants

Seed stocks	<i>Report on the source of all seed stocks or other plant material used. If applicable, state the seed stock centre and catalogue number. If plant specimens were collected from the field, describe the collection location, date and sampling procedures.</i>
Novel plant genotypes	<i>Describe the methods by which all novel plant genotypes were produced. This includes those generated by transgenic approaches, gene editing, chemical/radiation-based mutagenesis and hybridization. For transgenic lines, describe the transformation method, the number of independent lines analyzed and the generation upon which experiments were performed. For gene-edited lines, describe the editor used, the endogenous sequence targeted for editing, the targeting guide RNA sequence (if applicable) and how the editor was applied.</i>
Authentication	<i>Describe any authentication procedures for each seed stock used or novel genotype generated. Describe any experiments used to assess the effect of a mutation and, where applicable, how potential secondary effects (e.g. second site T-DNA insertions, mosaicism, off-target gene editing) were examined.</i>

ChIP-seq

Data deposition

- Confirm that both raw and final processed data have been deposited in a public database such as [GEO](#).
- Confirm that you have deposited or provided access to graph files (e.g. BED files) for the called peaks.

Data access links <i>May remain private before publication.</i>	<i>For "Initial submission" or "Revised version" documents, provide reviewer access links. For your "Final submission" document, provide a link to the deposited data.</i>
Files in database submission	<i>Provide a list of all files available in the database submission.</i>
Genome browser session (e.g. UCSC)	<i>Provide a link to an anonymized genome browser session for "Initial submission" and "Revised version" documents only, to enable peer review. Write "no longer applicable" for "Final submission" documents.</i>

Methodology

Replicates	<i>Describe the experimental replicates, specifying number, type and replicate agreement.</i>
Sequencing depth	<i>Describe the sequencing depth for each experiment, providing the total number of reads, uniquely mapped reads, length of reads and whether they were paired- or single-end.</i>
Antibodies	<i>Describe the antibodies used for the ChIP-seq experiments; as applicable, provide supplier name, catalog number, clone name, and lot number.</i>
Peak calling parameters	<i>Specify the command line program and parameters used for read mapping and peak calling, including the ChIP, control and index files used.</i>
Data quality	<i>Describe the methods used to ensure data quality in full detail, including how many peaks are at FDR 5% and above 5-fold enrichment.</i>
Software	<i>Describe the software used to collect and analyze the ChIP-seq data. For custom code that has been deposited into a community repository, provide accession details.</i>

Flow Cytometry

Plots

Confirm that:

- The axis labels state the marker and fluorochrome used (e.g. CD4-FITC).
- The axis scales are clearly visible. Include numbers along axes only for bottom left plot of group (a 'group' is an analysis of identical markers).
- All plots are contour plots with outliers or pseudocolor plots.
- A numerical value for number of cells or percentage (with statistics) is provided.

Methodology

- Sample preparation *Describe the sample preparation, detailing the biological source of the cells and any tissue processing steps used.*
- Instrument *Identify the instrument used for data collection, specifying make and model number.*
- Software *Describe the software used to collect and analyze the flow cytometry data. For custom code that has been deposited into a community repository, provide accession details.*
- Cell population abundance *Describe the abundance of the relevant cell populations within post-sort fractions, providing details on the purity of the samples and how it was determined.*
- Gating strategy *Describe the gating strategy used for all relevant experiments, specifying the preliminary FSC/SSC gates of the starting cell population, indicating where boundaries between "positive" and "negative" staining cell populations are defined.*
- Tick this box to confirm that a figure exemplifying the gating strategy is provided in the Supplementary Information.

Magnetic resonance imaging

Experimental design

- Design type *Indicate task or resting state; event-related or block design.*
- Design specifications *Specify the number of blocks, trials or experimental units per session and/or subject, and specify the length of each trial or block (if trials are blocked) and interval between trials.*
- Behavioral performance measures *State number and/or type of variables recorded (e.g. correct button press, response time) and what statistics were used to establish that the subjects were performing the task as expected (e.g. mean, range, and/or standard deviation across subjects).*

Acquisition

- Imaging type(s) *Specify: functional, structural, diffusion, perfusion.*
- Field strength *Specify in Tesla*
- Sequence & imaging parameters *Specify the pulse sequence type (gradient echo, spin echo, etc.), imaging type (EPI, spiral, etc.), field of view, matrix size, slice thickness, orientation and TE/TR/flip angle.*
- Area of acquisition *State whether a whole brain scan was used OR define the area of acquisition, describing how the region was determined.*
- Diffusion MRI Used Not used

Preprocessing

- Preprocessing software *Provide detail on software version and revision number and on specific parameters (model/functions, brain extraction, segmentation, smoothing kernel size, etc.).*
- Normalization *If data were normalized/standardized, describe the approach(es): specify linear or non-linear and define image types used for transformation OR indicate that data were not normalized and explain rationale for lack of normalization.*
- Normalization template *Describe the template used for normalization/transformation, specifying subject space or group standardized space (e.g. original Talairach, MNI305, ICBM152) OR indicate that the data were not normalized.*
- Noise and artifact removal *Describe your procedure(s) for artifact and structured noise removal, specifying motion parameters, tissue signals and physiological signals (heart rate, respiration).*

Volume censoring

Define your software and/or method and criteria for volume censoring, and state the extent of such censoring.

Statistical modeling & inference

Model type and settings

Specify type (mass univariate, multivariate, RSA, predictive, etc.) and describe essential details of the model at the first and second levels (e.g. fixed, random or mixed effects; drift or auto-correlation).

Effect(s) tested

Define precise effect in terms of the task or stimulus conditions instead of psychological concepts and indicate whether ANOVA or factorial designs were used.

Specify type of analysis: Whole brain ROI-based Both

Statistic type for inference

Specify voxel-wise or cluster-wise and report all relevant parameters for cluster-wise methods.

(See [Eklund et al. 2016](#))

Correction

Describe the type of correction and how it is obtained for multiple comparisons (e.g. FWE, FDR, permutation or Monte Carlo).

Models & analysis

n/a | Involved in the study

 Functional and/or effective connectivity Graph analysis Multivariate modeling or predictive analysis

Functional and/or effective connectivity

Report the measures of dependence used and the model details (e.g. Pearson correlation, partial correlation, mutual information).

Graph analysis

Report the dependent variable and connectivity measure, specifying weighted graph or binarized graph, subject- or group-level, and the global and/or node summaries used (e.g. clustering coefficient, efficiency, etc.).

Multivariate modeling and predictive analysis

Specify independent variables, features extraction and dimension reduction, model, training and evaluation metrics.